COMPONENTS' AND MATERIALS' PERFORMANCE FOR ADVANCED SOLAR SUPERCRITICAL CO2 POWERPLANTS

Performance in oxidizing and carburizing atmospheres: Characteristics and performance in regard to oxidation, corrosion, CO_2 in atmospheric and supercritical conditions, understanding the degradation mechanisms.

Deliverable Number 4.1

WP4 Evaluation and modelling of metal/medium interaction

Date: September 2023

Deliverable type: Report / **Dissemination level**: Public

Lead participant: Forschungszentrum Jülich

AUTHORS

Name	Organization
Florian Lebendig, Dmitry Naumenko	**FZJ**
Marta Navas, Elvira Oñorbe	**CIEMAT**
Otakar Frybort, Patricie Halodova	**CVR**
Emma White, Ceyhun Oskay	**DECHEMA**

DOCUMENT HISTORY

Version	Date	Change
01		Initial version uploaded

ABOUT THE PROJECT

COMPASsCO2 is a 4-year HORIZON2020 project started on 1.11.2020. It is led by the German Aerospace Center (DLR), with eleven additional partners from seven European countries.

COMPASsCO2 aims to integrate CSP particle systems into highly efficient s-CO_2 Brayton power cycles for electricity production. In COMPASsCO2, the key component for such an integration, i.e. the particle/s-CO_2 heat exchanger, is validated in relevant environments. To reach this goal, the consortium produces tailored particle and alloy combinations that meet the extreme operating conditions of the heat exchanger in terms of temperature, pressure, resistance to abrasion, oxidation and carburization. The proposed innovative particle CSP s-CO_2 Brayton cycle power plants will be flexible, highly efficient, cost-effective and 100% carbon neutral large-scale electricity generation facilities.

The research focus of COMPASsCO2 is on three main technological improvements: development of new particles, development of new metal alloys and development of the heat exchanger section.

DISCLAIMER

TABLE OF CONTENTS

LIST OF FIGURES

LIST OF TABLES

LIST OF ABBREVIATIONS

COMPASsCO2	Components' and Materials' Performance for Advanced Solar Supercritical CO2 Power Plants
FZJ	Forschungszentrum Jülich (Germany)
CIEMAT	Centre for Energy, Environmental and Technological Research (Spain)
DECHEMA	DECHEMA-Forschungsinstitut (Germany)
CVR	CENTRUM VYZKUMU REZ SRO (Czech Republic)
CST	Concentrating Solar Thermal
CSP	Concentrated Solar Power (Plants)
EC	European Commission
EU	European Union
IN740	INCONEL 740
IN617	INCONEL 617 (Alloy 617)
wt%	Weight percentage
SEM	Scanning Electron Microscopy
WP	Work package
EDX	Energy-dispersive X-ray spectroscopy
CO_2 4.5	Grade 4.5 = 99.995% purity

1   ABSTRACT

The Work Package 4 of the COMPASsCO2 project is mainly focused on assessment of candidate materials for particle/s-CO_2 heat exchangers. The laboratory tests are carried out under conditions simulating actual plant conditions. The degradation mechanisms of the materials are analysed and funnelled into a model in order predict operating lifetimes of the materials (heat carrier particles and heat exchanger components). Service lifetime estimation models of the interactions between particles degradation, alloys erosion and corrosion are being developed. The objectives are:

- To investigate the **oxidation**, **corrosion** and **wear** behaviour of the candidate materials
- To understand the degradation mechanisms
- To characterise the candidate materials and to assess their performance

The laboratory investigations include oxidation/corrosion and aim to understand the degradation mechanisms of these materials, in order to assess their performance. As the primary usage of these materials is in the heat exchanger of the innovative CSP-supercritical CO_2 power plants, separate investigations for each of the two atmospheres of the heat exchanger (ambient air and CO_2) were conducted.

Task 4.1 and Task 4.2 focused on investigating the material degradation on the outer side of the heat exchanger tubes (air oxidation) and the internal wall degradation (due to CO_2 corrosion). The investigations of oxidation and corrosion resistance were carried out in a test programme shared between FZJ, CIEMAT and CVR. The specimens were tested in air or CO_2 (technical or high-purity gas) at elevated temperatures (between 600°C and 900°C). The materials were characterised in thermogravimetry experiments (FZJ), quasi-isothermal oxidation (CIEMAT), and cyclic oxidation (FZJ), with future high pressure autoclave (CVR) tests planned. In order to evaluate the oxide scale growth kinetics and the microstructural changes in the materials induced by oxidation/corrosion, post-exposure characterisation was performed mainly by optical metallography and SEM/EDS analysis of cross-sections of the specimens.

The deliverable D 4.1 provides a comprehensive overview of the oxidation and CO_2-corrosion testing results.

2 ISOTHERMAL AND CYCLIC OXIDATION TESTING (FZJ)

2.1 GENERAL REMARKS

The isothermal and cyclic oxidation testing activities at FZJ included:

I. **Characterisation of as-received materials and sample pre-processing:** detailed chemical analysis of the candidate materials (especially for minor alloying elements and impurities known to have a profound effect on the oxidation resistance) and preparation of the sample for subsequent testing (refer to the following bullet points)

II. **Investigation of isothermal kinetics:** determination of the oxidation rates (k_p) in both air and CO_2 atmospheres; comprehensive analysis of the exposed samples: in metallographic cross-sections by optical metallography (and SEM/EDS)

III. **Cyclic oxidation testing:** with cycles consisting of 11 hours heating and 30 minutes cooling; determination of area specific weight changes in both air and CO_2 atmospheres at temperatures of 600°C, 700°C, and 900°C for a duration of 250 to maximum 3000 hours; complete analysis of the exposed sample materials: in metallographic cross-sections by optical metallography (SEM/EDS)

2.2 CHARACTERIZATION OF AS-RECEIVED MATERIALS

The study focused on the investigation of four commercial alloys, namely Sanicro 25, Alloy 617 (IN617), INCONEL 740 (IN740), and Haynes 282. These alloys are known for their exceptional high temperature properties and are designed for use in reheater and superheater tubes of power plants. IN617, IN740, and Haynes 282 are Ni-based alloys, whereas Sanicro 25 is an austenitic alloy. As a reference material at lower temperatures (maximum 600°C), a ferritic-martensitic steel P92 was also investigated. FZJ performed a chemical composition analysis of the material batches used as detailed in Table 1.

Table 1. Compositions (wt.%) of investigated state-of-the-art materials as determined by ICP-OES and combustion analysis for non-metals.

Alloy	Fe	Ni	Co	Cr	Al	Mo	Ti	Mn	Si	C	Other
Sanicro 25	41.5	24.2	1.50	23.4	0.03	0.23	0.03	0.56	0.19	0.084	Cu 2.93, Nb 0.5 W3.47, N 0.28
Alloy 617	1.03	51.9	11.9	22.1	1.16	9.0	0.39	0.09	0.32	0.076	W 0.32
IN740	0.15	48.0	21.4	25.2	1.35	0.53	1.49	0.30	0.18	0.048	Nb 1.5, Ce 0.12
Haynes 282	0.61	52.5	10.1	18.6	1.50	8.7	2.15	0.05	0.25	0.070	Ce 0.17
P92	84.6	0.34	0.017	9.37	-	0.38	-	0.57	0.22	0.150	W 1.74, V 0.22

The etched metallographic cross-sections of the as-received materials are given in Figure 1, showing the microstructures typical for the respective materials in recrystallized and annealed conditions.
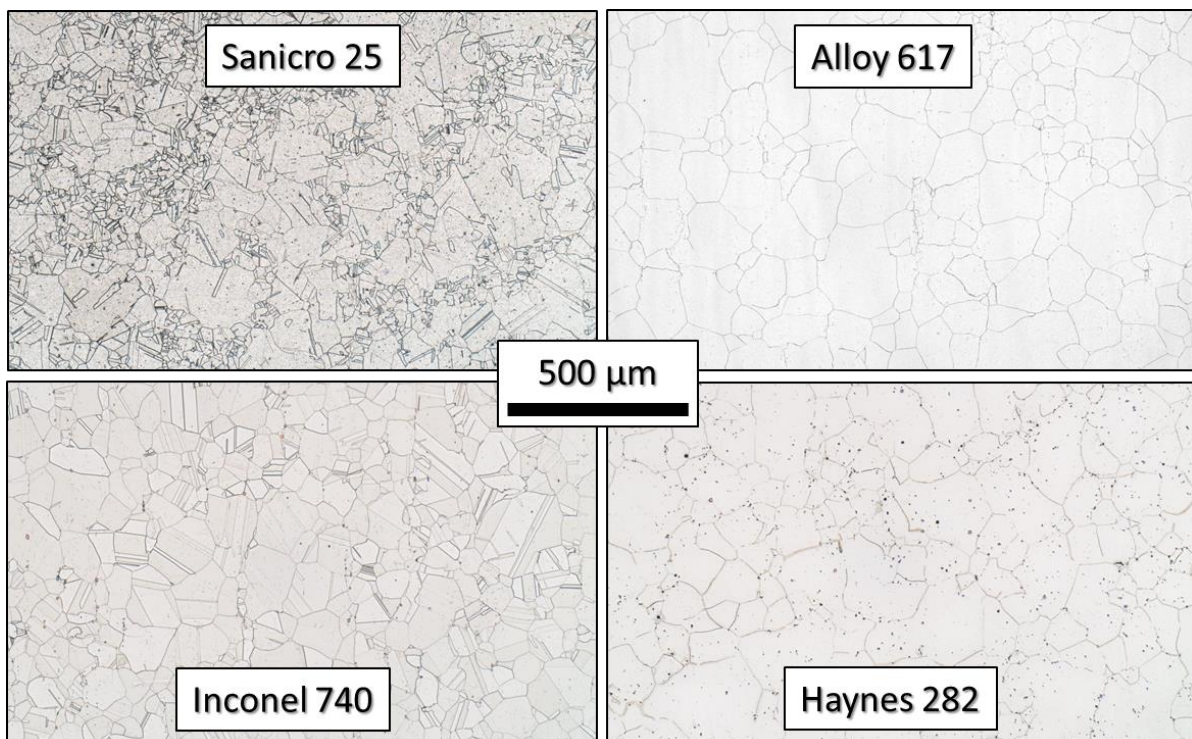
Figure 1. Etched metallographic cross-sections of as-received materials.

2.3 SPECIMEN PREPARATION

The specimens investigated in this study (as listed in Table 1) had dimensions of 20 × 10 × 2 mm, and were cut from the received plate and tube materials. Prior to further investigations, they were ground using a P1200 grit surface finish and cleaned ultrasonically in ethanol.

2.4 TESTING PROCEDURES

2.4.1 Thermogravimetry experiments

The oxidation exposures were carried out at 700°C and 900°C in ambient air and technical CO_2 (99.995% purity) at atmospheric pressure in order to assess the oxidation performance of the alloys. Short-time isothermal oxidation exposures at 600°C, 700°C, 800°C, and 900°C were conducted for 72 hours using a SETARAM thermobalance to accurately measure the oxidation kinetics in air and CO_2. The specimens were suspended in the TGA-furnace using alumina holders. The gas flow rate was 2 l/h. The heating rate was 90 K/min and cooling rate 10 K/min, respectively.

2.4.2 Cyclic oxidation testing

The automated cyclic oxidation rigs utilized for cyclic oxidation exposures in both air and CO_2 atmospheres are shown in Figure 2. The specimens on a holder were moved into the hot zone of the furnace for 11 hours and moved out for cooling for 30 minutes in order to reach a maximum hot time per day, thereby shortening the overall test time. Specimens were weighed at regular time intervals, i.e. after 44 hours hot-time increments.

(a)   **(b)**

Figure 2. Automated air cyclic oxidation test rig (a) and CO_2 cyclic oxidation test rig (b).

2.4.3 Post-test sample processing and microstructural analyses

Exposed specimens were processed for further investigations using metallography, and sample cross-sections were prepared. The sample coupons were cut into two pieces of approximately 10 × 10 × 2 mm in size at the same location as shown in Figure 3. Following this, the specimens were sputtered with a thin gold layer to impart electrical conductivity and electrochemically coated with a nickel layer of approximately 20 µm in thickness in order to protect the specimen surface from damage during the next preparation steps. The specimens were then embedded in an epoxy resin. SiC paper was used for grinding and diamond pastes were used to polish down to 1 µm surface finish. Colloidal SiO_2 slurry was used for a final polishing step.
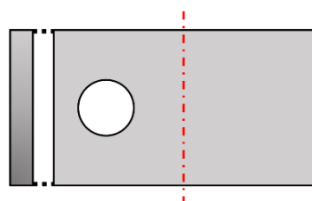
Figure 3. Schematic representation of 20x10x2 mm specimens used at FZJ for oxidation and CO_2-corrosion tests. Red dashed lines indicate locations of metallographic cross-section analysis.

2.5 INVESTIGATION OF ISOTHERMAL KINETICS

Figure 4 shows the mass changes obtained during isothermal exposure in the thermobalance. The data reveal that the oxidation for all of the investigated alloys obeyed a parabolic rate law for the examined time range up to 72 hours at 900°C. In both test gases mass changes increased in the order of: Sanicro 25 < IN617 < IN740 < Haynes 282. Table 2 illustrates the parabolic oxidation rates calculated from the mass changes correspondingly also increase in this same order.

The oxidation rates were found to be increased for the alloys when exposed in CO_2, and the effect appeared to be independent of the material. However, for Haynes 282 the effect is comparatively the weakest.

Table 2. Determined k_p values in $g^2/(cm^4 \cdot s)$ for the alloys exposed in air or CO_2 (4.5) for 72 hours at 900°C.

Alloy	Air	Technical grade CO_2
Sanicro 25	6.71×10^{-13}	1.03×10^{-12}
IN617	5.54×10^{-13}	1.09×10^{-12}
IN740	9.36×10^{-13}	1.33×10^{-12}
Haynes 282	2.47×10^{-12}	2.89×10^{-12}

(a)

(b)
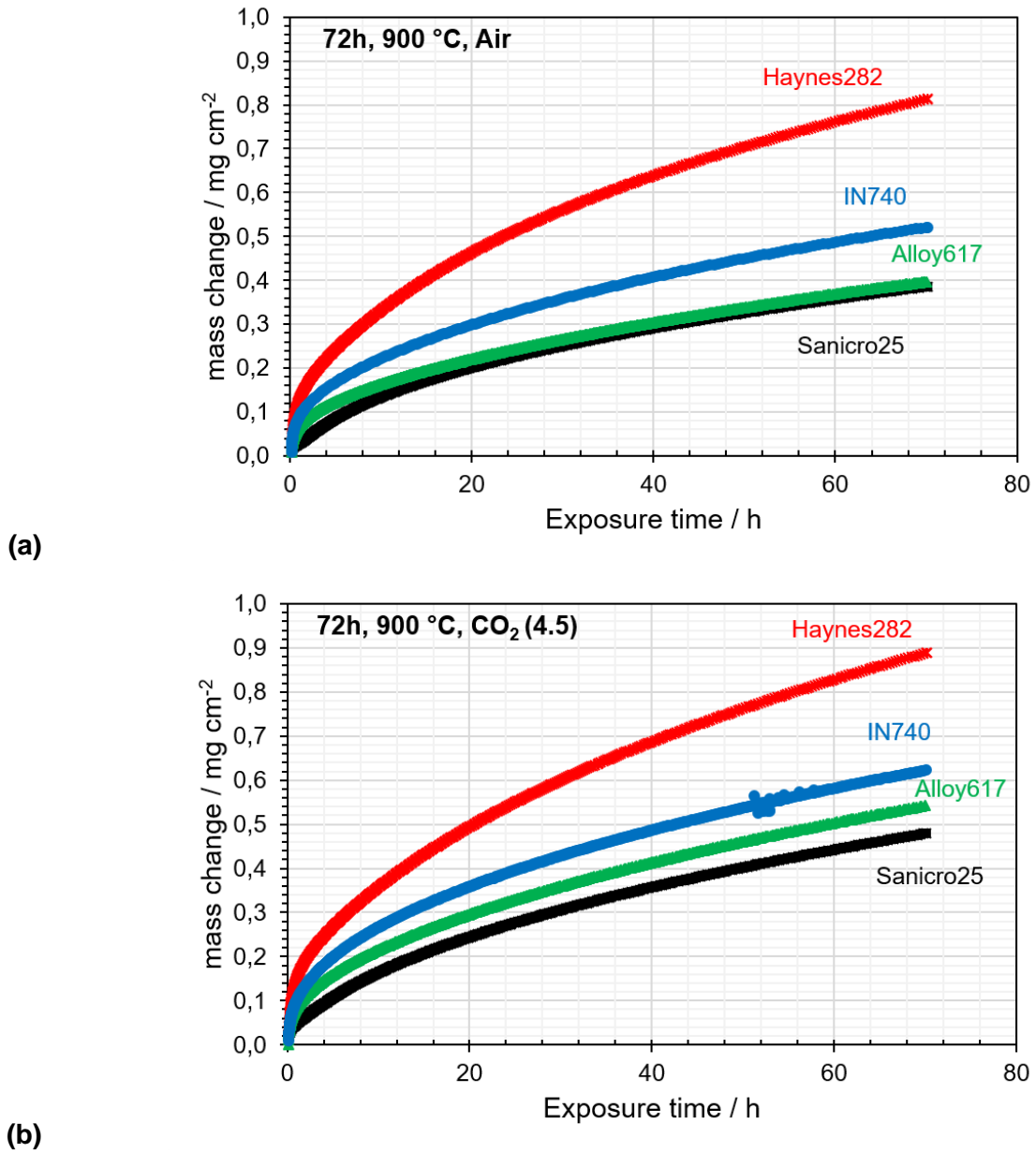
Figure 4. Relative weight changes of Haynes 282, IN740, IN617, and Sanicro 25 during isothermal oxidation exposure in air (a), and in CO2 (4.5) (b) for 72 hours at 900°C.

Figure 5 displays backscattered electron images depicting a thicker oxide scale on Haynes 282, with the lowest scale thickness observed on Sanicro 25 after exposure in both environments. The Ni-base alloys also exhibited internal oxidation of Al, which is an additional reason for their higher mass changes when compared to Al-free Sanicro 25. This observation is consistent with the mass change data shown in Figure 4.
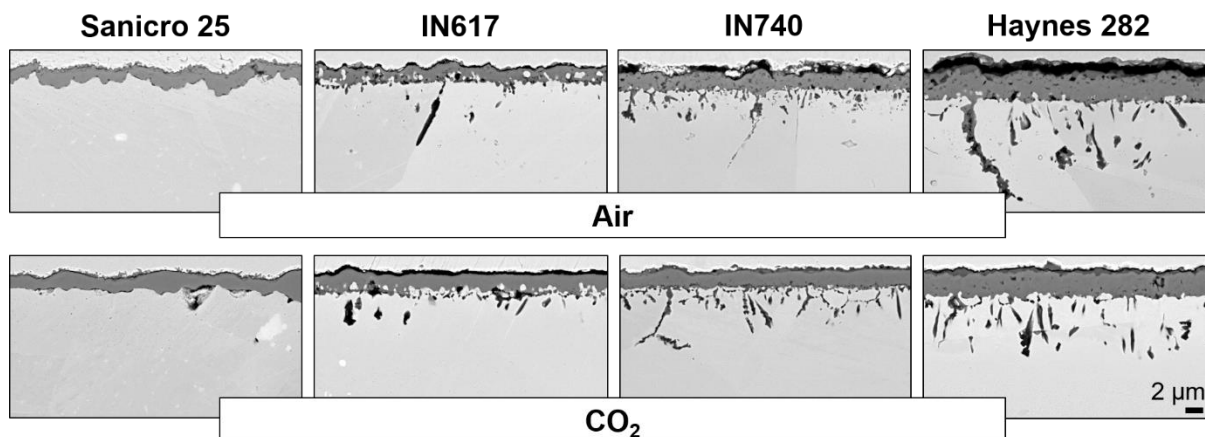
Figure 5. Backscattered electron images of cross-sectioned candidate materials after isothermal oxidation exposures for 72 hours at 900°C in air and CO_2.

2.6 CYCLIC OXIDATION TESTING

Cyclic exposures were conducted in air and CO_2 at 900°C and are illustrated in Figure 6.
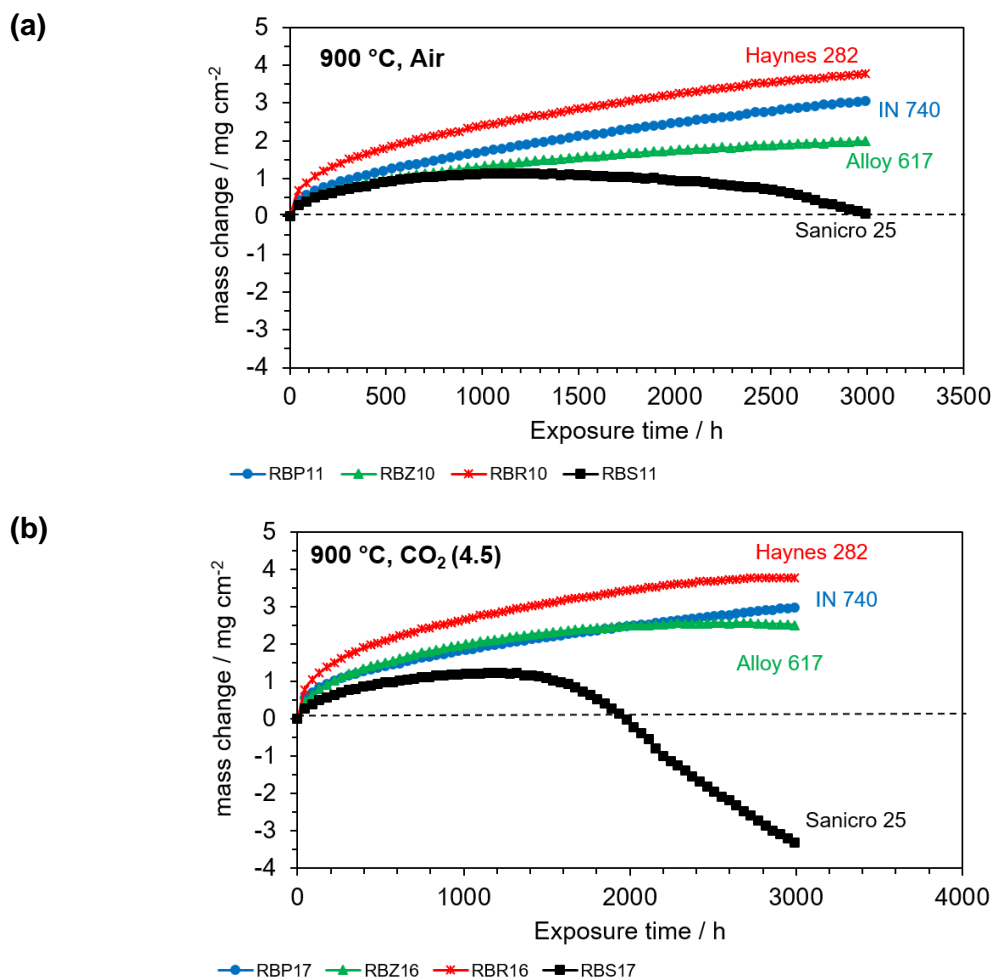

Figure 6. Relative weight change of Haynes 282, IN740, IN617, and Sanicro 25 during cyclic oxidation exposure in air (a), and in CO_2 (4.5) (b) for 3000 hours at 900°C.

The mass change data in Figure 6 after short durations are in agreement with the mass changes obtained during isothermal oxidation (compare with Figure 4). Haynes 282 shows the highest mass gains, Sanicro 25 the lowest, IN740 and IN617 exhibit intermediate values.

After longer exposure, Sanicro 25 exhibits a decrease in mass. The effect seems to be stronger in CO_2 when compared to air (compare oxidation rates, k_p, in Table 2). IN617 started to exhibit slightly decreasing mass changes at about 2500 hours in CO_2. Under these test conditions, the decreasing mass change is typically related to oxide scale spallation.

Figure 7 shows cross-sections of the studied alloys after cyclic oxidation at 900°C for 1000 hours. All alloys formed Cr_2O_3 oxide scales and the Ni-base alloys additionally had zones of Al internal oxidation. Backscattered electron images of the cross-sectioned alloys are consistent with the mass change data presented in Figure 6.

Figure 8 compares EDS results with SEM images and corresponding Ti-maps (showing Ti-enrichment in the oxide scale) for exposures in both atmospheres, air and CO_2. This enrichment increased in the order of IN617 – IN740 – Haynes 282. The Ti-enrichment in the scale increases with increased Ti content (compare with Table 1). The distribution of Ti is remarkable. All alloys exhibited Ti enrichment on the oxide surface. For the alloys with higher Ti contents (IN740 and Haynes 282), the enrichment of Ti was also observed in the inner part of the scale and/or in the internal oxidation zone. For the same alloy, no apparent difference in the enrichment of Ti in the oxide scale was observed when comparing the two different atmospheres.

The Ni-base alloys showed internal oxidation of Al below the scales. The extent of the internal oxidation increases with increased Al content (compare Figure 7 and Table 1).

IN617 exhibited TiN precipitate formation after cyclic oxidation exposure in air, but no such precipitates were found within the matrix after exposure in CO_2.
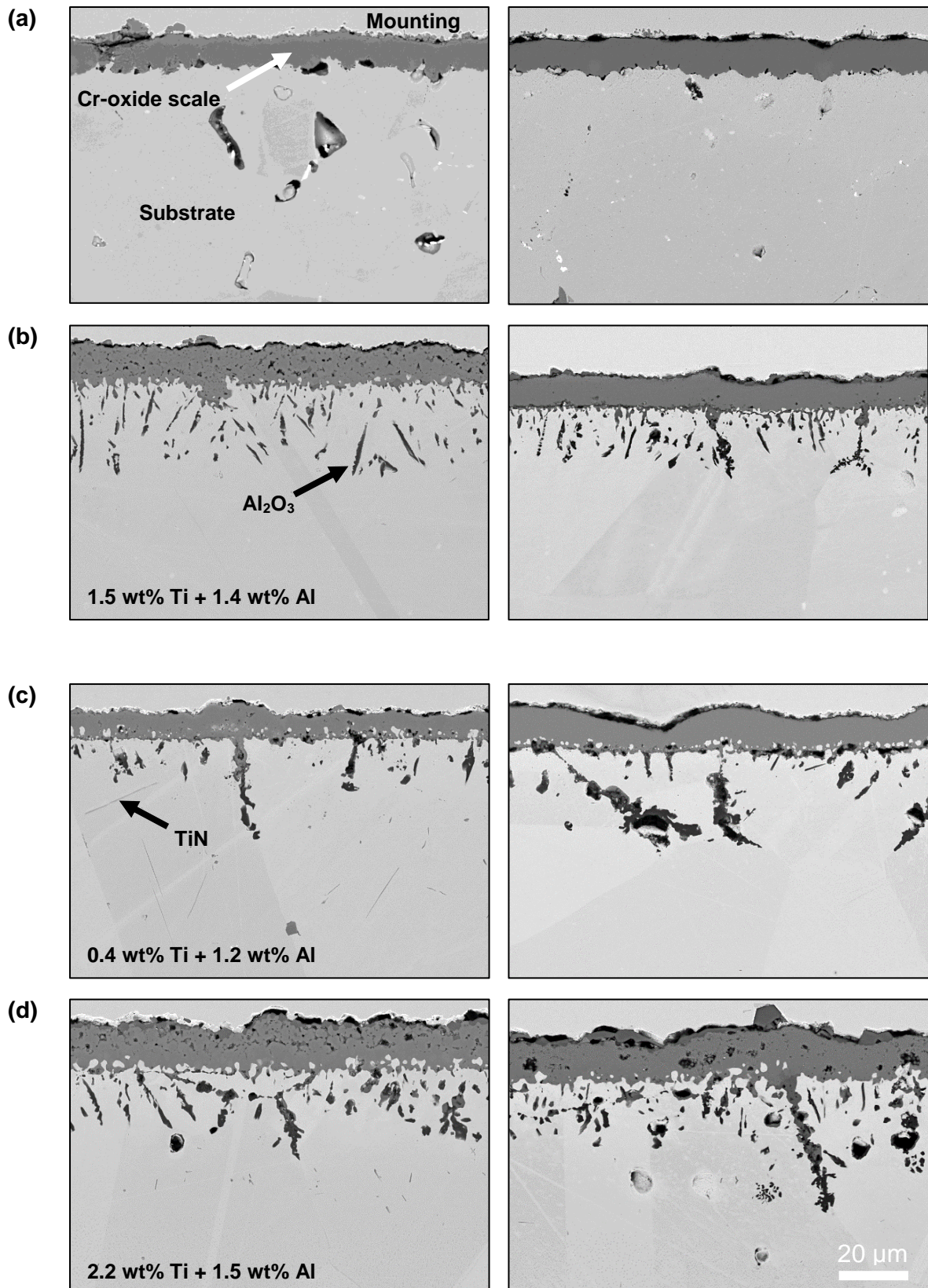
Figure 7. Backscattered electron images of cross-sectioned Sanicro 25 (a), IN740 (b), IN617 (c), and Haynes 282 (d) after cyclic oxidation exposures for 1000 hours at 900°C in air (left column) and CO_2 (right column).
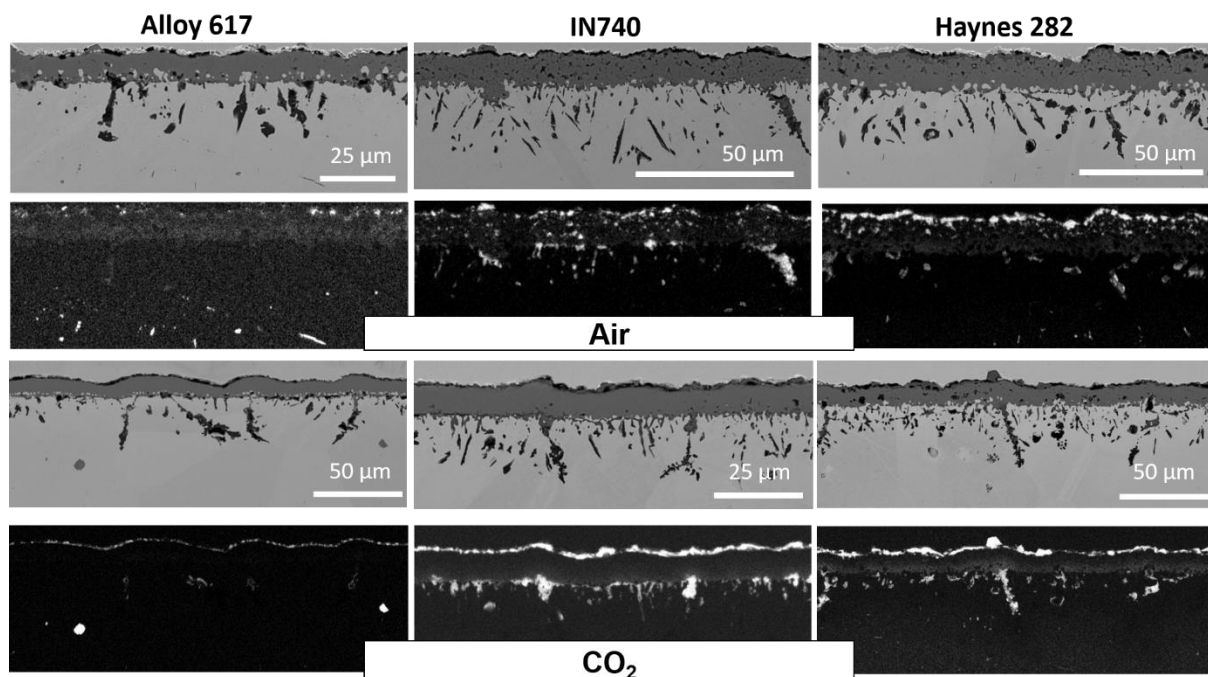
Figure 8. Backscattered electron images of cross-sectioned Alloy 617, IN740, and Haynes 282 with corresponding EDX maps (Ti Kα1) showing Ti-enrichment in the oxide scale after cyclic oxidation exposures for 1000 hours at 900°C in air (first two rows) and CO_2 (last two rows).

Notably, the oxide scale of Haynes 282 remained intact after 3000 hours of exposure in air, whereas Sanicro 25 exhibited evident regrowth after spallation, as depicted in Figure 9. This observation is in agreement with the mass change data in Figure 6 showing substantial mass loss from Sanicro 25.
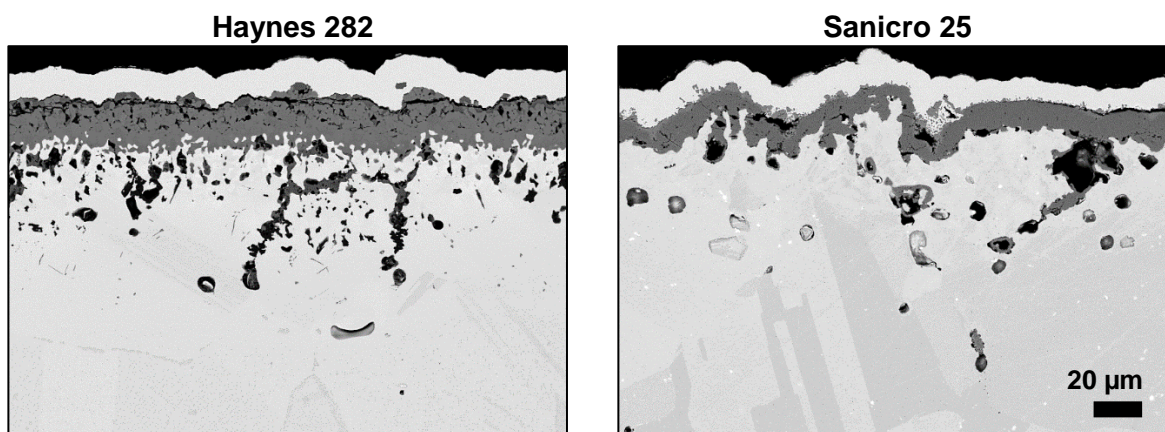
Figure 9. Backscattered electron images of cross-sectioned Haynes 282 and Sanicro 25 after cyclic oxidation exposures for 3000 hours at 900°C in air.

Table 3 summarizes the data obtained from the image analysis of the cross-sections in Figure 7. The data refer to exposures at 900°C in CO_2 (4.5) (prior to macroscopically visible spallation).

Table 3. Correlation of mass changes and cross-section images analysis data (refer to Figure 7, right column, exposure in CO_2).

Alloy		Average scale thickness (cross-section) in μm	Mass change calculated from measured scale thickness* in mg cm^{-2}	Mass change measured after oxidation testing in mg cm cm^{-2}	Calculated mass change due to internal oxidation in mg cm^{-2}
Sanicro 25		8.4	1.4	1.1	-/-
IN617		10.2	1.7	1.8	0.1
IN740		9.3	1.6	1.8	0.2
Haynes 282		12.3	2.1	2.6	0.5

* assuming 1 mg cm^{-2} mass change corresponds to 6 μm of flat Cr_2O_3 scale thickness

It can be seen that the higher mass change of Haynes 282 can only partly be related to the increased internal oxidation. To a significant extent, the chromia scale formed on Haynes 282 is thicker than that on the other studied alloys.

2.7 DISCUSSION OF OXIDATION MECHANISMS

Previous studies have revealed that titanium accelerates the growth of chromia scales (Cruchley, Evans, Taylor, Hardy, & Stekovic, 2013). Ti is supposed to be incorporated into Cr_2O_3, leading to increased growth by p-type doping, i.e. Ti^{4+}ions substituting Cr^{3+}ions, which results in the formation of Cr cation vacancies, which leads to faster cationic diffusion transport through the scale (Young, 2008). This enhancement however likely reduces over time because of Ti depletion in the alloy.

Based on the present results, a greater oxide spallation was observed for Sanicro 25 as compared to the other Ni-base alloys. This observation was somewhat unexpected considering that the Ni alloys had higher oxide scale growth rates and thicker scales are more typically prone to spallation. This phenomenon can only be partially attributed to a higher coefficient of thermal expansion (CTE) of Sanicro 25 (17.5x10^{-6} 1/K in T=30-900°C) compared to Haynes 282 (15.9x10^{-6} 1/K in T=30-900°C), because the CTE-difference is only about 10%. One possible explanation is that the difference in the oxide microstructures plays a role. The fast growing scales containing defects (vacancies, pores) on IN740 and Haynes 282 are likely to have a lower modulus of elasticity resulting in less stress generation upon the same thermal mismatch strain induced between the oxide and metal upon cooling. Another possible explanation for better scale adherence on Haynes 282 and IN740 is the presence of minor Ce additions in their analysed compositions, as evident from Table 1 (note Ce was not specified in the nominal chemical compositions). Ce plays a crucial role in augmenting the properties of Ni and Co-based alloys at high temperatures by enhancing their oxidation resistance. The addition of RE (reactive elements) such as Ce to alloys is expected to getter the alloy detrimental impurities, in particular sulphur. Gettering of sulphur prevents void formation and oxide adherence loss associated with the segregation of the latter impurity to the oxide-metal

interface. It is noteworthy that IN617, without a reactive element addition, showed slight weight losses at the end of 3000 hours exposure in the CO_2 atmosphere, possibly indicating initial spallation.

No substantial differences in the oxide scale growth rates were found between exposures in air and CO_2 under the tested conditions (at atmospheric pressure). Moreover, no indications for internal carburization were seen from the SEM cross-sectional analysis. At the same time internal nitride formation was observed in the cross-sections meaning that the oxide scales on the Ni-based alloys were permeable to nitrogen. This observation indicates that the oxide scale growth occurs by a mechanism not involving access of CO_2 molecules to the oxide/metal interface. This could be predominant cation transport and/or (partial) oxygen ion transport through the scale, presumably at the grain boundaries, the oxygen being supplied by dissociation of CO_2 according e.g. to the reaction:

$$CO_2 = CO + \tfrac{1}{2} O_2 \qquad\qquad (1)$$

The relatively slow consumption of oxygen associated with slow growth rates of the chromia scales on the surface of the specimens, compared to the availability of the flowing test gas in the reaction tube, ensures that the composition of the gas phase was unchanged during the test.

3   ISOTHERMAL LONG-TERM CO$_2$ EXPOSURES (CIEMAT)

3.1 GENERAL REMARKS

The activities at CIEMAT included:

   I.   Characterisation of as-received materials and sample preparation for testing
   II.   Long term thermal oxidation tests with CO$_2$ at atmospheric pressure
   Thermal oxidation tests are performed up to 5000h or 3000h, at 7000 and 900°C respectively, in order to determine the oxidation rates, by means of weight gain measurements metallographic and post-test examination and the characterization of oxide layer using SEM EDX and XPS spectroscopy. The objectives of these tests are to study the following:

   -   Effect of the quality of CO$_2$ gas with two different commercial purities: research and industrial grade
   -   Effect of temperature with oxidation tests at 700 and 900 °C
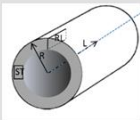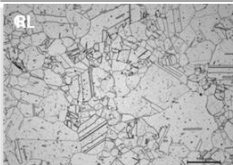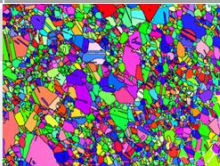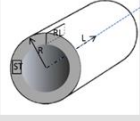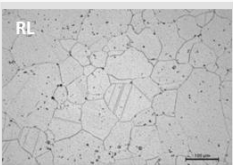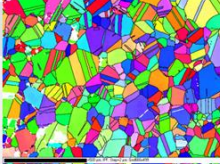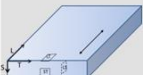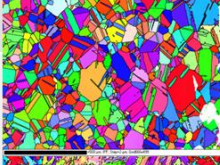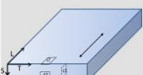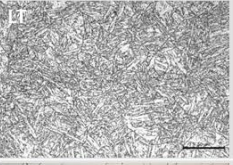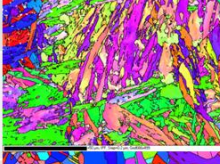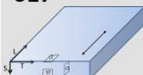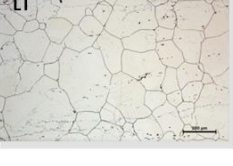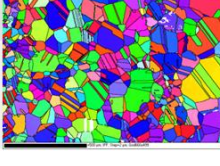
3.2 CHARACTERIZATION OF AS-RECEIVED MATERIALS

The study is focused on the investigation of the same four commercial alloys of other partners, namely Sanicro 25, Alloy 617 (IN617), INCONEL 740 (IN740), and Haynes 282 (Table 1). As it was above mentioned, these alloys are known for their exceptional high temperature properties. Sanicro 25 is an austenitic alloy while the rest of the materials are Ni-based alloys, IN617, IN740, and Haynes 282.

The initial microstructure of the SOA materials has been characterized by means of OM and SEM/EBSD. The main results are shown in Table 4 and can be summarized as follows:

- P92 is a ferritic/martensitic steel with a large prior austenitic grains were martensitic laths are preferentially oriented within primary austenite grains (PAGs).

- Sanicro 25 is an austenitic steel with a bimodal grain size distribution and no preferential orientation of grains.

- Haynes 282, I740 and I617 are Ni-base alloys with a similar grain size with a random orientation.

- Vickers hardness has been also measured being higher for Ni-base alloys (I740>H282≥I617), followed by P92 and Sanicro 25.

- Ti-rich precipitates are observed in Ni-base alloys with other alloying elements (Mo, Nb).

Table 4 Microstructural characterization of as-received SOA Materials

Material	OM	Grain size (ASTM E-112)			Hardness (HV)			SEM/EBSD
SANICRO 25		ST	RL		ST	RL		
		-	6.5		182±13	201±8		
HAYNES 282		ST	RL		ST	RL		
		3.8	3.4		221±14	244±14		
INCONEL 740		LT	ST	LS	LT	ST	LS	
		4.4	4.0	4.1	358±22	366±54	323±17	
P92		LT	ST	LS	LT	ST	LS	
		-	-	6.7	209±78	235±5	227±7	
INCONEL 617		LT	ST	LS	LT	ST	LS	
		2.8	3.4	3.3	218±36	219±58	224±47	

3.3   SPECIMEN PREPARATION

The materials were received in the form of plates and tubes (H282 and S25) from where the specimens to be tested were machined. An example for Sanicro 25 is shown in Figure 10. The specimens investigated in this study had dimensions of 25 × 12 × 3 mm. All the specimen surfaces were ground using a 1200 Grit surface finish and cleaned ultrasonically in ethanol.
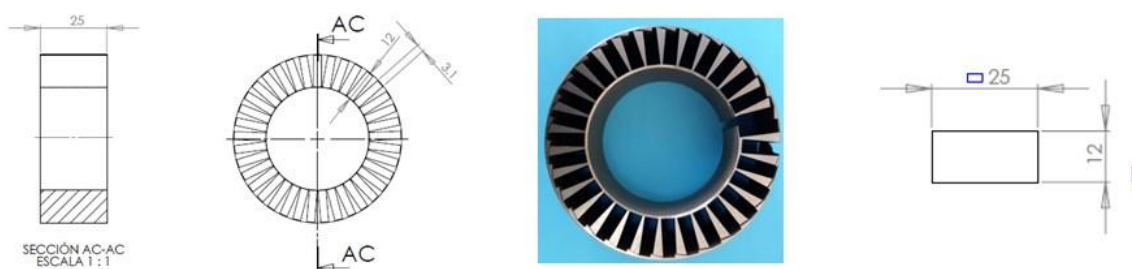
Figure 10: Specimens preparation of Sanicro 25

3.4   TESTING PROCEDURES

Long-term thermal oxidation tests have been performed in tubular furnaces with closed quartz tubes at high temperatures (700 and 900 °C) with a CO_2 atmosphere (Figure 11). Tests are carried out at atmospheric pressure with a constant controlled flow of CO_2 gas. The samples are located in a specific ceramic support shown in Figure 11. Weight gain measurements of the specimens were measured every 500 h up to the end of the tests. Some specimens were removed at intermediate stop in order to perform the post-test characterization to study the time evolution of the material defects and the oxide layers composition.
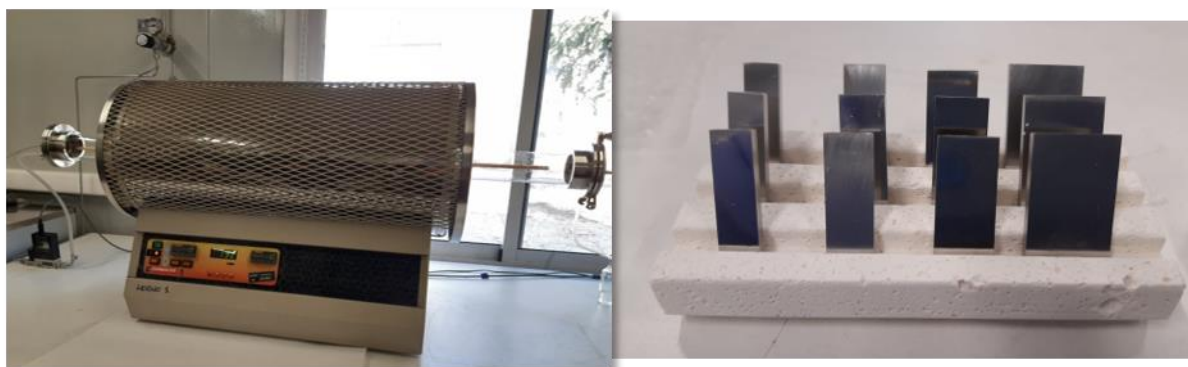
Figure 11: Tubular furnace with closed quartz tube and specimens with ceramic support.

The effect of CO_2 qualities was studied, in the long term tests at 700°C up to 5000h, using industrial (IG) and research (RG) grades of commercial CO_2. Table 5 shows the composition of the two grades with differences on water and oxygen content. The industrial grade used at Ciemat had similar composition of the CO_2 atmosphere used by other partners.

Table 5: CO_2 grades composition

Identification		Purity	Composition (ppm)					
			O_2	H_2O	N_2	C_nH_m	CO	H_2
Research grade	4.8	99.998	<2	<3	<8	<2	<1	<0.5
Industrial grade	N38 (≈4.5)	99.98	<10	<10		<5		

Effect of temperature was studied by the comparison of the oxidation/corrosion results obtained at 700 and 900°C, using the industrial grade of CO_2, with the same materials up to 3000h testing.

Post-test examination included the characterization of one specimen of each material tested at the different conditions and exposure times: 500h, 1000h, 3000h and 5000h. Each metallographic specimen was examined to detect and characterize the material degradation along the longitudinal sections of the specimens. Cross sections of the tested materials were studied by means of Scanning Electron Microscopy (SEM) and Energy Dispersive x-ray Spectroscopy (EDS) to determine the formation and composition of the oxide layer, internal oxidation and precipitates present in the matrix. In addition, the oxide layer were analyzed by means of X-ray photoelectron Spectroscopy (XPS) to determine the depth profile of chemical composition and to study the evolution with the exposures times.

3.5 RESULTS AND DISCUSSION

3.5.1 Effect of CO_2 quality (700 °C)

Weight gain measurements of the materials tested at 700 °C under the two qualities of CO_2 (IG and RG) were measured every 500 h up to 5000 hours testing, and the results are shown in Figure 12. Under each CO_2 quality, there is a clear difference between the materials tested. Haynes 282 weight gains are higher than the rest of materials, followed by Inconel 617B and 740 with similar trend between them, and Sanicro 25 presents the lowest value. These results on weight gain could be associated with the titanium content (Table 1) following the trend: H282>I740≥I617B>S25.

The weight gain evolution with long-term exposures shows that the corrosion kinetic follows a parabolic law in all the materials tested, as it was expected for the alloys forming protective oxide scales.

According with the Figure 12, no significant differences were observed comparing the results of the two grades of commercial CO_2. This result is relevant for the design of the system and can play an important role in the cost of the operation of the power plant. In addition, the results obtained in the tests of the different laboratories are also comparable between them.
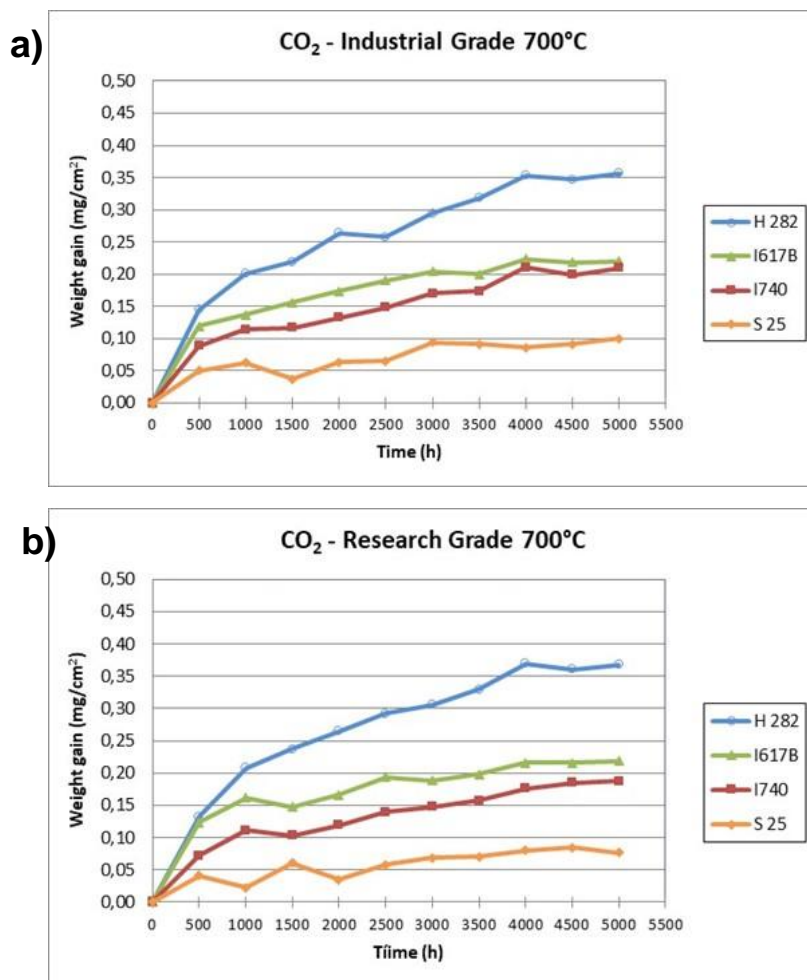
Figure 12: Weight gain measurements at 700 °C for Sanicro 25, Inconel 740, Inconel 617B and Haynes 282 under CO2 atmosphere: a) IG and b) RG

Figure 13 shows images of the evolution of the oxide layer for the studied materials (Sanicro 25, Inconel 617B, Inconel 740 and Haynes 282) tested at 700 ºC under IG CO_2 atmosphere at 500, 1000, 3000 and 5000 hours. In the case of specimens tested at 1000, 3000 and 5000h a nickel layer was deposited over oxide layer in order to protect them.

All the materials showed an increase in the thickness of the oxide scales with increasing exposure time in agreement to weight gain measurements. Comparing the different materials, the thicker oxide layer after 5000 h of exposure time corresponds to Haynes 282, followed by I617B and I740, and Sanicro 25 with the thinner oxide layer.

Internal oxidation zones were detected below the oxide layer in the specimens of Ni-base alloys. The internal oxidation increases with increasing the alloy Al content.
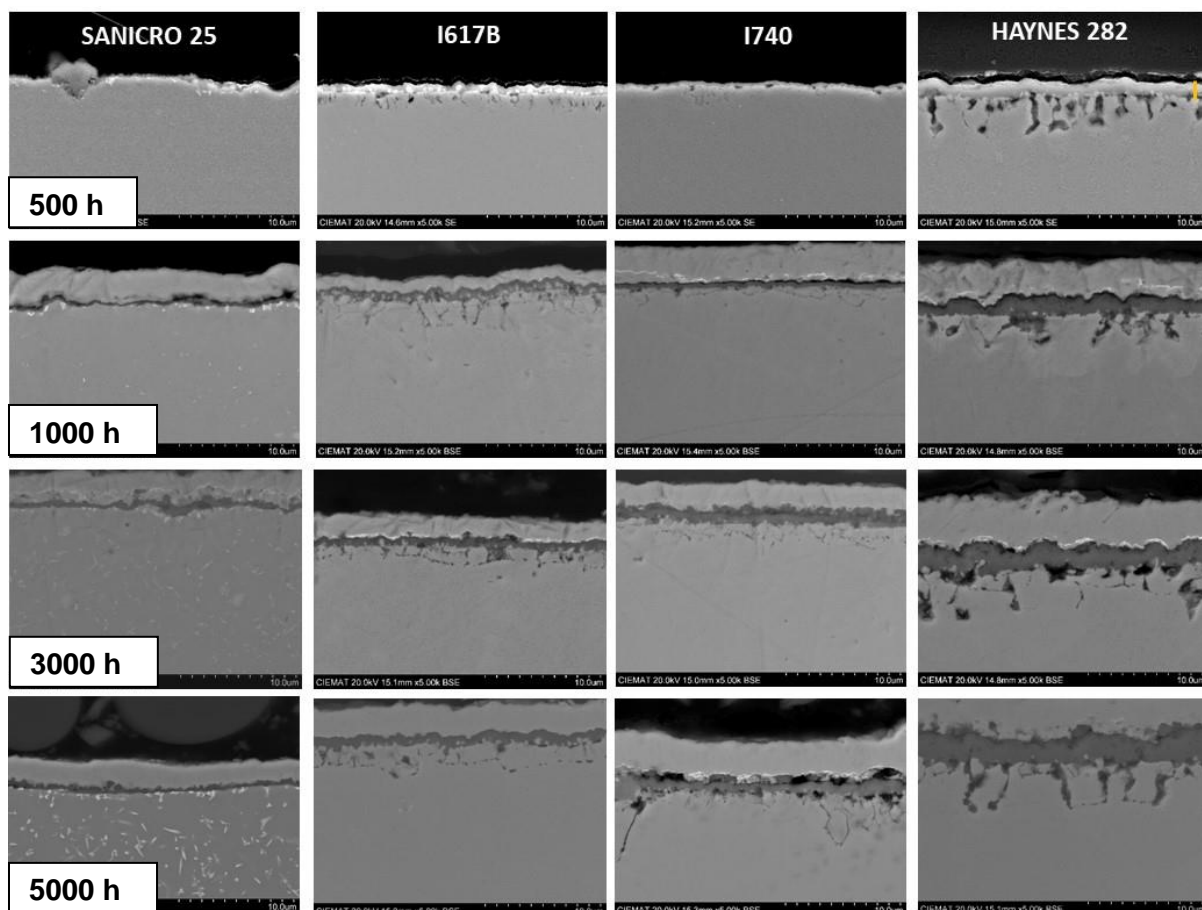
Figure 13: SEM images of the oxide layer of the different materials tested in atmospheric CO$_2$ (IG) at 700 ºC

EDS results of the materials tested at 700 ºC during 5000 h are shown in Figure 14. The scale in the inner part contains mainly Cr and Mn oxides. Underneath the oxide layer there is a depletion of Cr in all the materials. An internal oxidation zone was detected below the oxide layer in the specimens of Ni-base alloys. This internal oxidation of Inconel 617B is detected by the presence of oxygen and aluminum while the titanium can be observed as islands of precipitates. On the contrary, the internal oxidation of Inconel 740 and Haynes 282 is correlated with aluminum and titanium. In both materials, the titanium is also present in the outer oxide layer. The thickness of the oxide and the internal oxidation is greater for Haynes 282 and Inconel 740, according to the titanium content of the alloy.
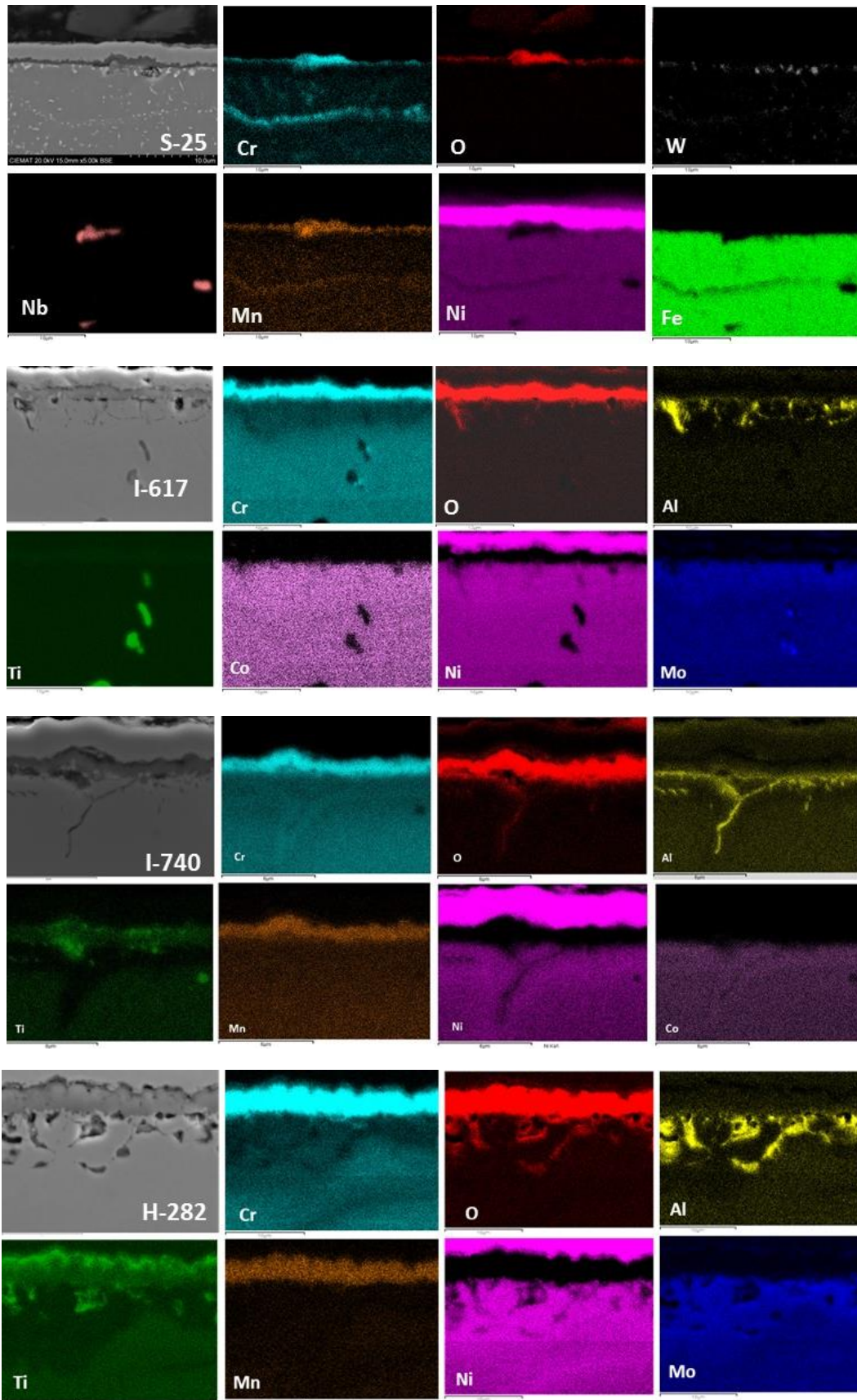
Figure 14: EDS mapping of materials tested in atmospheric CO_2 (IG) at 700 ºC during 5000h

X-ray photoelectron Spectroscopy (XPS) was employed to study the evolution of the composition of the oxide layer in the studied materials after 500 h and 5000 h of exposure time at 700 ºC under IG and RG CO_2 qualities although only results for IG are presented because no significant differences where observed (Figure 15). The depth profile of the oxide layer are in accordance with EDS observations. The oxide layers are mainly composed by Cr in all the materials and an outer thin oxide with Ti and/or Mn depending on the concentration of these alloying elements in each material. Furthermore, Al was also detected after long exposures in the case of Ni-base materials (black line in Figure 15 b).
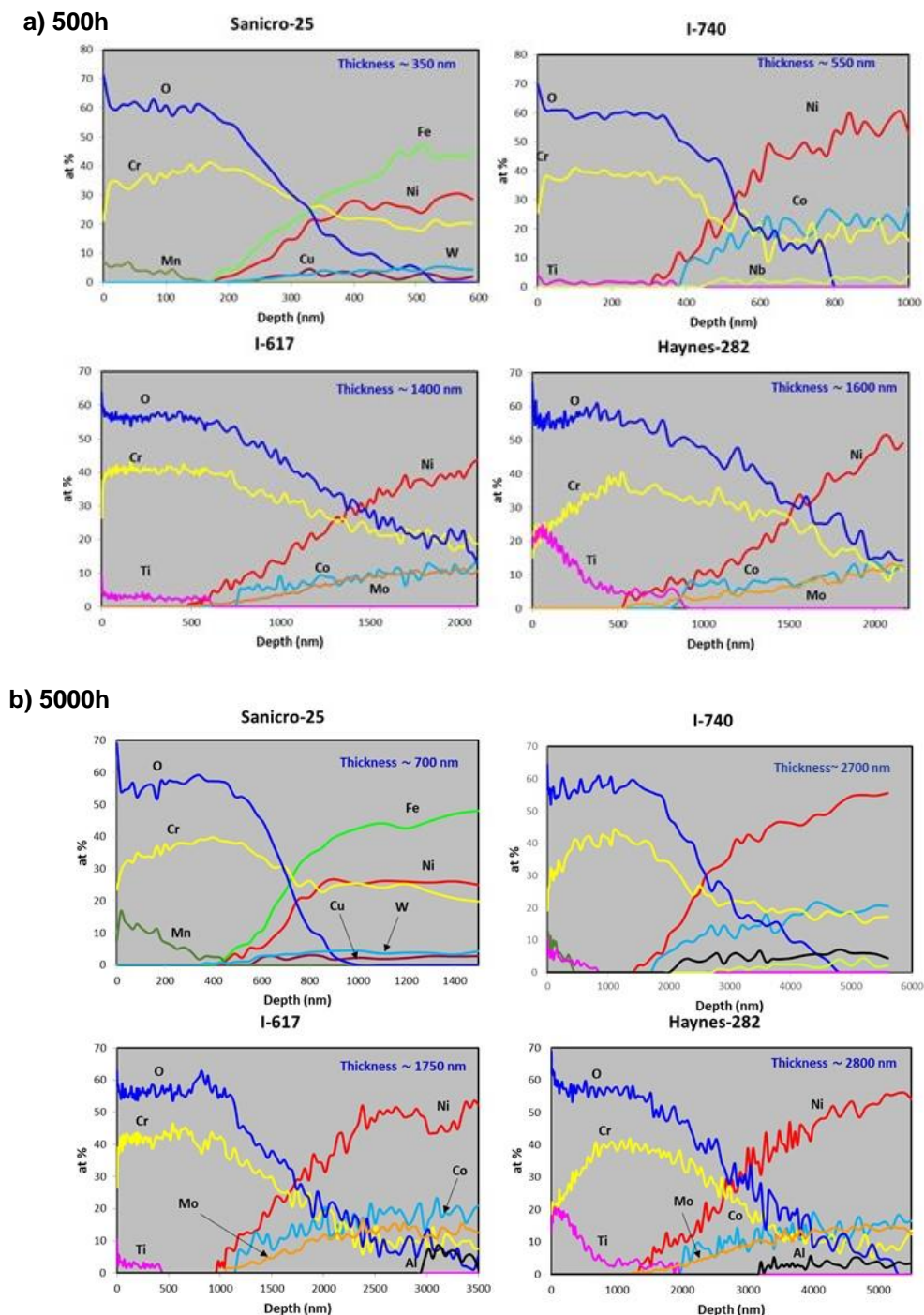
Figure 15: XPS depth profiles for the different materials tested in atmospheric CO_2 at 700 ºC during a) 500 h and b) 5000 h.

Table 6 summarizes the thickness of the oxide scales obtained by SEM-EDS and XPS spectroscopy. The XPS thickness is determined as the point in which oxygen concentration reduces to 50 % of the oxygen concentration at the plateau. Similar values were obtained in both techniques and the growth oxide layer with time is in accordance with the increase of thickness with the Ti content of the alloy, as it was concluded with the weight gain measurements.

Table 6: Oxide layer thickness of specimens tested at 700 °C.

MATERIAL	700 °C, time	Thickness SEM (µm)	Thickness XPS (µm)
Sanicro 25	500 h	0.6	0.5
Inconel 617B		1.3	1.5
Inconel 740		0.7	0.7
Haynes 282		1.8	2.1
Sanicro 25	1000 h	0.6	
Inconel 617B		1.3	
Inconel 740		0.7	
Haynes 282		2.1	
Sanicro 25	3000 h	1.1	
Inconel 617B		2.3	
Inconel 740		2.7	
Haynes 282		3.0	
Sanicro 25	5000 h	1.4	0.7
Inconel 617B		2.5	1.8
Inconel 740		2.4	2.7
Haynes 282		4.8	2.8

3.5.2 Temperature effect (700 °C IG vs 900 °C IG)

Since no differences between the two CO_2 grades were observed in previous tests at low temperature, the tests at 900 °C were only performed using industrial grade CO_2 atmosphere.
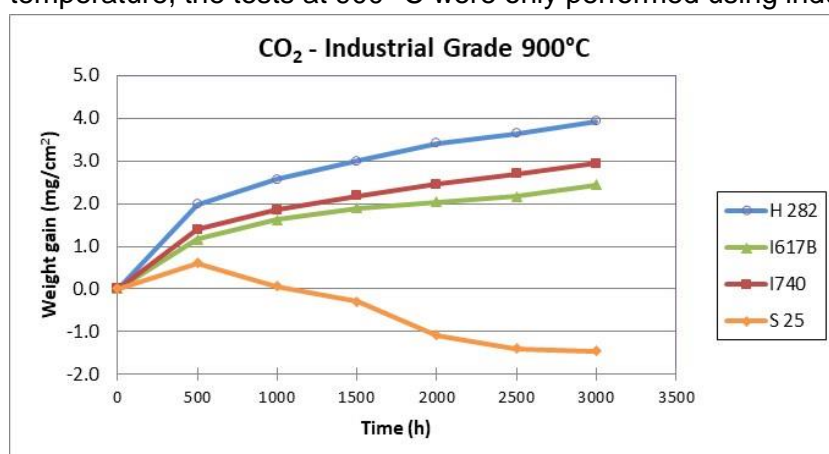
Figure 16 shows the weight gain measurements obtained at 900 °C.
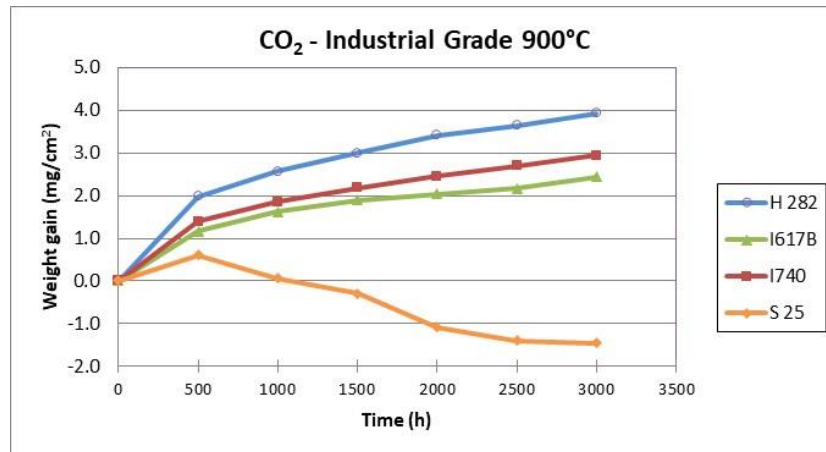
Figure 16: Weight gain measurements for Sanicro 25, Inconel 740, Inconel 617B and Haynes 282 under IG CO_2 atmosphere at 900 °C.

The effect of the temperature is clearly observed in the case of nickel base alloys (Haynes 282 and 617B and 740 Inconel) because the weight gains are one order of magnitude greater than specimens tested at 700 °C (Figure 12 a). At 900 °C, Haynes 282 also shows higher values than Inconel alloys with similar values between them.

In the case of the Sanicro 25, the material behavior is clearly different due to a decrease of weight gains after 500 hours testing, even with negative values. Such a behavior can be associated with formation of poorly adherent oxide scales prone to spallation from the metal upon cooling.

Figure 17 shows the SEM images of the oxide layers of the materials after 500 and 1000 h exposure at 900°C. As was expected and in agreement with the weight gain measurements, the oxide scales are significantly thicker than those formed at the lower temperature, even in the case of Sanicro 25.
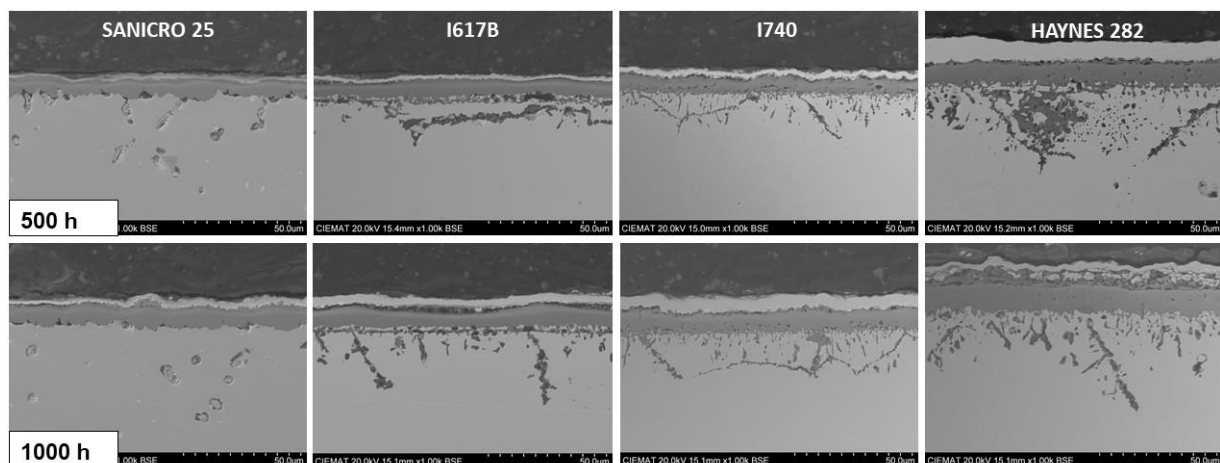

Figure 17: SEM images of the oxide layer of the different materials tested in atmospheric CO_2 (IG) at 900 ºC during 500 h and 1000h.

The measurements of the maximum oxide scale thickness detected by SEM are shown in Table 7. The thicknesses of Ni-base alloy are one order of magnitude higher than those obtained at 700ºC (Table 6) and the differences between materials are maintained: H282>I740≥I617B, in agreement with the weight changes. On the contrary, the thickness of the Sanicro 25 oxide layer is similar to that of the other materials despite the spallation signs

deduced from the gain measurements. This fact points to the need to determine the weight loss measurements that are being performed for all the materials and conditions tested.

Table 7: Oxide layer thickness of specimens tested at 900 °C

MATERIAL	900 ºC, time	Thickness SEM (µm)
Sanicro 25		10.2
Inconel 617B	500 h	10.8
Inconel 740		11.6
Haynes 282		14.4
Sanicro 25		10.0
Inconel 617B	1000 h	10.8
Inconel 740		16.9
Haynes 282		17.5

Figure 18 shows the EDS cross-section maps after exposures at 900°C.
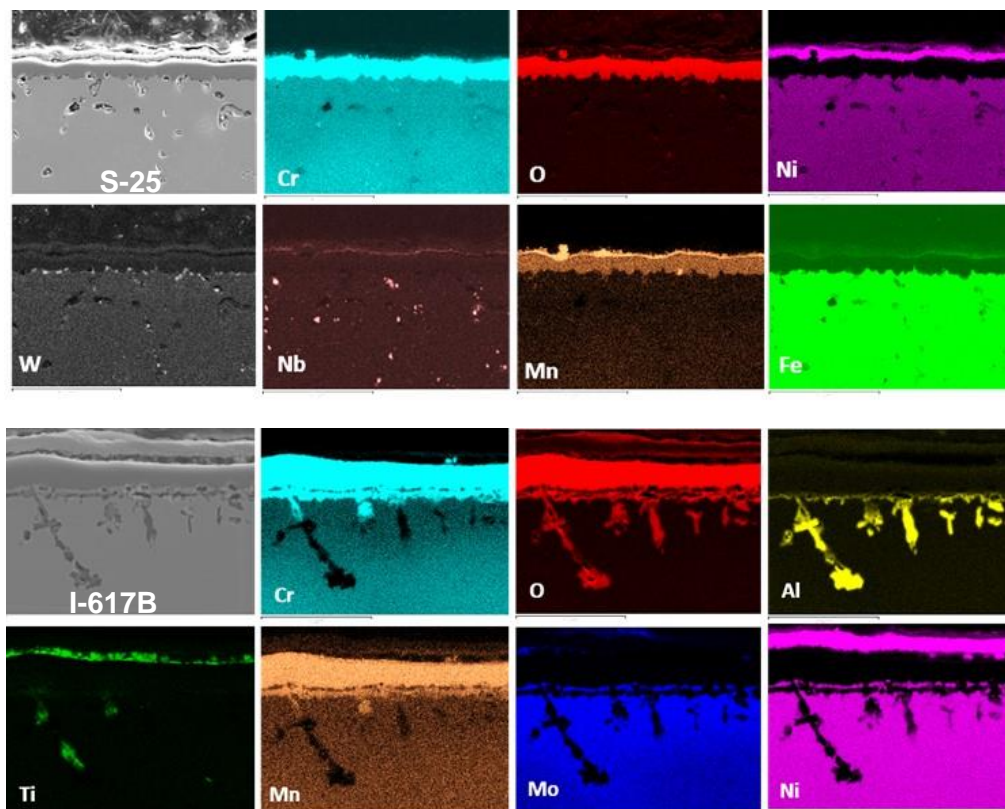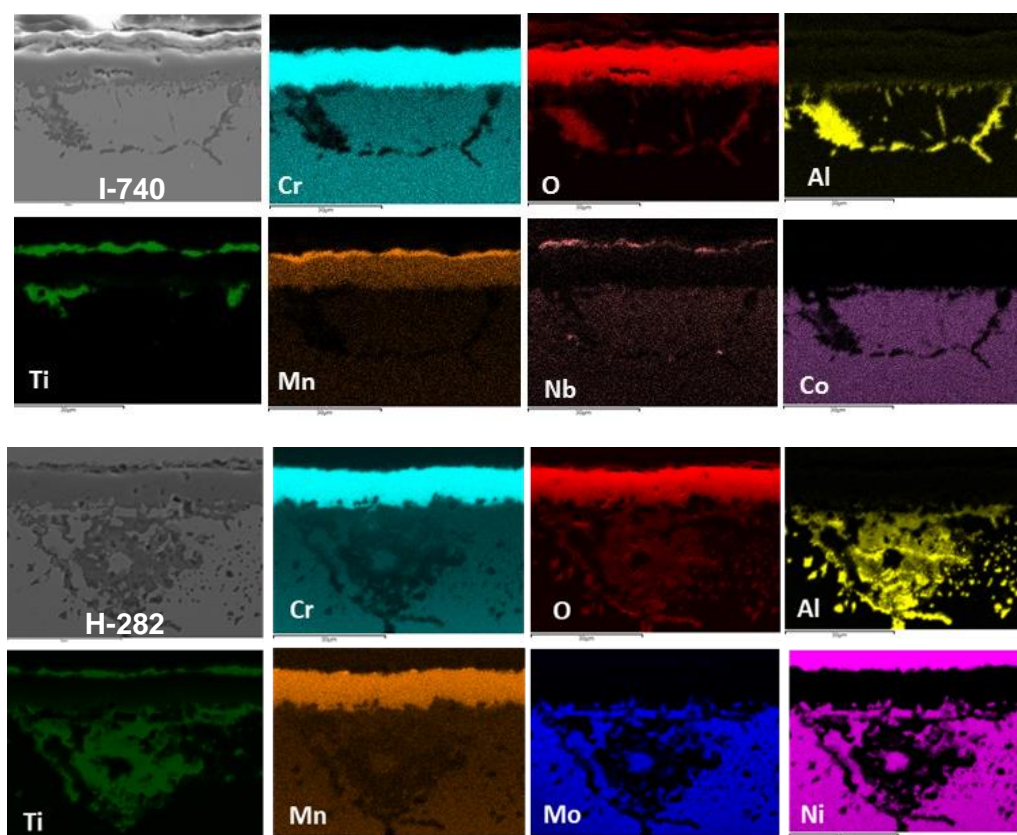
Figure 18. EDS mapping of materials tested in atmospheric CO_2 (IG) at 900 ºC during 500h.

The compositions of the reaction products are similar to those obtained at 700 ºC although in the former case the oxide scales are thicker and the depths of internal oxidation are greater, in agreement with the mass change measurements.

Sanicro 25 has not shown internal oxidation and the oxide scales formed present an outer thin oxide layer enriched in manganese and inner oxide rich in chromium and manganese. Small W-rich inclusions seem to precipitate below the oxide layer.

Nickel base alloys show an outer oxide layer of titanium and thicker inner layer rich in chromium and manganese. Under the oxide film, an internal oxidation zone of titanium and aluminum is observed that seems to be located predominantly at the grain boundaries. The thickness of the internal oxidization zone increases with temperature and the titanium and aluminium contents of the alloy, being the greatest in Haynes 282. Other minor alloying elements are also present within the oxide scales, such as niobium in the case of Inconel 740. All of these results will be confirmed with the XPS analyses of oxide layer at long times.

The chemical composition of oxide and internal oxidation layers agree with results obtained by other authors (Perez-Gonzalez F., 2014) in dry oxidation of Haynes 282 at high temperatures. These authors concluded that external oxides of TiO_2 and Cr_2O_3 layers results from the migration of Cr and Ti ions from the base material while internal oxides of TiO_2 and Al_2O_3 results from the oxidation of the respective metallic elements originally present in gamma prime precipitates $Ni_3(Al,Ti)$.

4   TESTING UNDER SUPERCRITICAL CONDITIONS (CVR)

To describe the corrosion behaviour of candidate materials of heat exchanger at simulated operating conditions, Supercritical Carbon dioxide Autoclave (ScCAc) system was assembled at CVR. Corrosion tests in flowing supercritical CO_2 at high temperature will be carried out on specially prepared material samples.

4.1 SCCAC DEVICE FOR TESTING

Supercritical Carbon dioxide Autoclave (ScCAc) experimental device is based on a two-stage principle with high-pressure side (pump, autoclave vessel, heat exchanger and cooler) and low-pressure side with storage tank and measurements, which can maintain continuous flow of sCO_2 over the specimen area. Pressure is raised with three head piston pump and regulated with backpressure regulator. The temperature of the vessel is set by external furnace controlled by central Control unit with DAQ capabilities for all sensors.

Main parameters of the system:

Max. temperature: 700 °C

Max. pressure: 25 MPa

Max. flow: 3 l.h-1
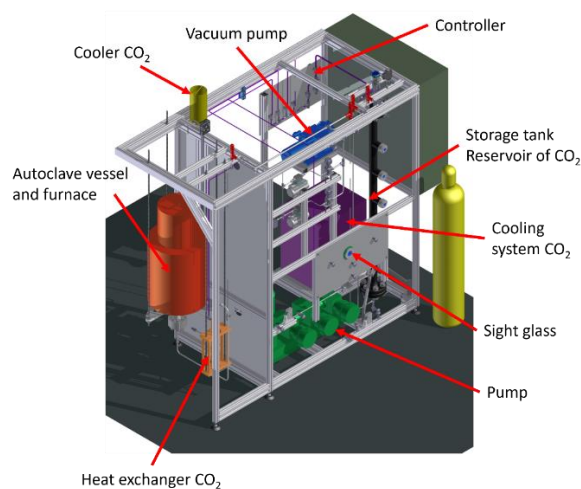
Figure 19. Supercritical Carbon dioxide Autoclave model with the description of the main components (left), the current state of the assembled device during the test operation (right).

4.2 SCO2 CORROSION TESTING

After the test runs expected high temperature corrosion tests in sCO_2 will be performed. Weight Loss Coupons (WLC) from state of the art (SOTA) materials (Sanicro 25, IN 617, IN 740, Haynes 282) were machined in CVR workshops by EDM machining according to the cutting scheme, developed for each type of as-received material. After the machining, the cleaned samples were further polished with SiC paper to create a homogenous surface finish of 600 grit. Moreover, test specimens of the novel materials of Cr, Cr-Ni-Al and Cr-Ni-Al-Fe alloys and the applied Cr-Si diffusion coatings on SOTA materials were received for testing. In

order to expose large number of prepared specimens (up to 100 pcs), a new test section sample holder was designed and manufactured, made of IN625 with a coating of TiAlSiN (Marvin™).

Corrosion testing parameters will be set to:

Temperature: 700 °C

Pressure: 120 bar

Gass purity: I.G. (99.995) CO_2 (Linde supply)

Expected test duration: 1000 hours for novel materials, 3000 hours for SOTA materials

4.3 POST-TESTING MATERIALS CHARACTERIZATION

In order to evaluate the materials after the sCO_2 exposure, detailed microstructural characterization will be performed to identify the corrosion mechanisms, estimate the corrosion rates and characterize the processes of materials degradation. The post-test characterization will include gravimetry, metallography, LOM, SEM-EDX, XRD and supplementary GDOES analytical techniques.

5   SUMMARY AND CONCLUSIONS

Based on the results obtained, the following conclusions can be drawn regarding the oxidation and CO_2 corrosion behaviour.

- The scale growth rate during cyclic oxidation in air and industrial grade CO_2 correlated with the alloy Ti content and the extent of internal oxidation increased with increasing the alloy Al content.
- Indications for a higher tendency for scale spallation in CO_2 when compared to air were observed; more extensive scale spallation occurred for Sanicro 25 (S25), in spite of a low scale growth rate. It is likely the high coefficient of thermal expansion and absence of reactive elements, which can improve the scale adherence or significantly reduce the parabolic scaling rate, had an impact.
- The oxide scales formed during cyclic oxidation were only slightly thicker in CO_2 when compared to air for the Ni-base alloys and Sanicro 25.
- The weight gain measurements during discontinuous exposures of the different materials at 700 °C and 900°C in atmospheric pressure CO_2 are correlated with the titanium content of the alloys in the following order: H282 > IN740 ≥ IN617B > S25.
- Oxidation tests with two grades of CO_2 (lower purity industrial and higher-purity research grades) have not shown significant differences in the weight gains and chemical composition and thickness of the oxide. This result is relevant for the design of the system and can play an important role in the operation cost of the power plant.
- Effect of the temperature is clearly observed in the case of nickel base alloys (Haynes 282 and 617B and IN740). The weight gains at 900 °C are one order of magnitude greater than those of the specimens tested at 700 °C. At 900 °C, Haynes 282 also

shows higher weight gains than Inconel alloys (IN617B and IN740 with similar values between them).

- The tests at longer times, specially up to 5000 h, showed that the corrosion/oxidation kinetics follow a parabolic law with relatively small weight gains at longer times. This behavior is expected considering formation of protective oxide scales.

- Nickel base alloys formed oxide scales with an outer layer rich in titanium and thicker inner layer of chromium and manganese rich oxides. Underneath the oxide scales, internal oxidation zones are observed consisting of Ti and Al-rich oxide precipitates that appear to be located predominantly at the alloy grain boundaries. The internal oxide penetration increases with the temperature and the titanium and aluminium contents of the alloy, and is especially pronounced in the case of Haynes 282.

- In the case of Sanicro 25 tested at 900°C, the measured specific weight decreased after 500 hours testing. This behavior may be related to the formation of a poorly adherent oxide scale leading to its spallation upon cooling.

6 FUTURE WORK

Testing with novel CrSi and Cr-Ni-Al based alloys and coatings have been initiated under the same test conditions as described in the current report. The above presented data with the state-of-the-art alloys will be used as a reference to qualify the resistance to air oxidation and CO_2 corrosion of the newly developed materials. At CVR high-pressure sCO_2 tests will be performed.

7 REFERENCES

Cruchley, S., Evans, H. E., Taylor, M. P., Hardy, M. C., & Stekovic, S. (2013). Chromia layer growth on a Ni-based superalloy: Sub-parabolic kinetics and the role of titanium. *Corrosion science, 75*, 58–66.

Galiullin, T., Gobereit, B., Naumenko, D., Buck, R., Amsbeck, L., Neises-von Puttkamer, M., & Quadakkers, W. J. (2019). High temperature oxidation and erosion of candidate materials for particle receivers of concentrated solar power tower systems. *Solar Energy, 188*, 883–889.

Huczkowski, P., Ertl, S., Piron-Abellan, J., Christiansen, N., Höfler, T., Shemet, V., . . . Quadakkers, W. J. (2005). Effect of component thickness on lifetime and oxidation rate of chromia forming ferritic steels in low and high pO2 environments. *Materials at high temperatures, 22*, 253–262.

Kofstad, P. (1988). High Temperature Corrosion, Elsevier Applied Science. *London, 211p.*

Liu, H.-N., Nomura, M., Ogi, K., & Sakamoto, M. (2001). Abrasion resistance of high Cr cast irons at an elevated temperature. *Wear, 250*, 71–75.

Migas, D., Myalska-Głowacka, H., Chmiela, B., Maciąg, T., Mikuszewski, T., Moskal, G., . . . Godzierz, M. (2022). Microstructural characterization of cerium rich phases in new

polycrystalline Co–Al–W-xCe superalloys. *Journal of Materials Research and Technology, 20*, 1665–1676.

Young, D. J. (2008). *High temperature oxidation and corrosion of metals* (Bd. 1). Elsevier.

Perez-Gonzalez F., Garza Montes de Oca, Colás R. (2014) High emperature chracterization ofthe Haynes 282 Ni-based superalloys. Oxid Met, 82, 145-161